Analyst

Cite this: *Analyst*, 2011, **136**, 3349

www.rsc.org/analyst

PAPER

TiO_2-decorated graphene nanohybrids for fabricating an amperometric acetylcholinesterase biosensor

Kun Wang,* He-Nan Li, Jun Wu, Chang Ju, Jia-Jia Yan, Qian Liu and Baijing Qiu

Received 21st March 2011, Accepted 24th May 2011
DOI: 10.1039/c1an15227k

This work describes a highly sensitive and rapid amperometric biosensor for organophosphate compounds (OPs) based on immobilization of acetylcholinesterase (AChE) on a novel TiO_2-decorated graphene (TiO_2-G) nanohybrid, which was constructed by *in situ* growth of TiO_2 nanoparticles (NPs) on the graphene sheet. The well-dispersed TiO_2 NPs eliminated the restacking of TiO_2-G nanohybrids. Due to the integrating of TiO_2-G nanohybrids, the as-prepared biosensor showed high affinity to acetylthiocholine (ATCl) with a Michaelis–Menten constant (K_m) value of 0.22 mM, and rapid inhibition time (3 min). Further, based on the inhibition of OPs on the enzymatic activity of the immobilized AChE, and using carbaryl as a model compound, the inhibition of carbaryl was proportional to its concentration ranging from 0.001 to 0.015 and 0.015 to 2 μg mL^{-1} with a detection limit of 0.3 ng mL^{-1} (S/N = 3). The developed biosensor exhibited a good performance for organophosphate pesticide detection, including good reproducibility and acceptable stability, which provided a new and promising tool for the analysis of enzyme inhibitors.

Introduction

Organophosphate compounds (OPs), as the most commonly applied pesticides in agriculture, are typical examples exhibiting fairly high toxicity. With the exploitation of many new pesticides, the rapid determination and reliable quantification of trace levels of these compounds are significant to health and the environment.[1] A combination of enzymatic reactions with the electrochemical method allows the development of different enzyme-based electrochemical biosensors for environmental analysis.[2] Among these, amperometric acetylcholinesterase (AChE) biosensors have shown satisfactory results for OPs determinations based on the inhibition of AChE,[3,4] in which the enzyme activity was employed as an indicator for quantitative measurement of insecticides. When AChE is immobilized on the working electrode surface, its interactions with the substrate of acetylthiocholine (ATCl) produce the electroactive product of thiocholine. The inhibition on the enzyme system can be monitored by measuring the oxidation current of thiocholine.[2] As an alternative strategy, quite a lot of advanced nanomaterials, such as gold nanoparticles (AuNPs) and carbon nanotubes (CNTs), have been employed for AChE biosensors fabrication, which showed good performance including high sensitivity, rapid response and good stability.[5–7]

Key Laboratory of Modern Agriculture Equipment and Technology, School of Chemistry and Chemical Engineering, Jiangsu University, Zhenjiang, 212013, China. E-mail: wangkun@ujs.edu.cn; Fax: +86 511 8791708; Tel: +86 511 8791800

Graphene-based hybrids with metals, metal oxides and polymers have received increasing attention during recent years, due to these hybrids affording significant physicochemical properties by effective adjustment or interaction of graphene sheets and incorporated materials.[8,9] Several graphene hybrids have been elaborately designed, prepared, and further applied in electrochemical biosensors,[10] because of the inherent properties of graphene sheets including high surface area, excellent thermal conductivity and electric conductivity, strong mechanical strength, *etc*.[11] Besides, the functionality of the incorporated materials also makes a contribution to these graphene hybrids. Recently, both Niu's and Ramaprabhu's groups fabricated Au/graphene nanohybrids by a chemical reduction method, and further respectively exploited the development of electrochemical biosensor.[12,13] Raj's group prepared the hybrid material derived from nanoscale Pt particles and graphene, and further developed a highly sensitive amperometric cholesterol biosensor.[14] Our group has confirmed the enhanced direct electrochemistry of glucose oxidase (GOD) by employing nanohybrids of graphene with CdS as an immobilization matrix.[15] Compared with wide applications of the CNT-based nanohybrid for fabricating varieties of biosensors,[16,17] it is just the beginning for graphene-based nanohybrids with more excellent physicochemical properties in the field of electrochemical biosensors.[10]

Meanwhile, semiconductor nano-sized TiO_2 has been extensively used in a wide range of applications due to its non-toxicity, long term stability, low cost, multifunctions and good biocompatibility.[18] Particularly, the utilization of various carbonaceous materials, such as mesoporous carbon and carbon nanotubes,[19,20] as the building block of the TiO_2-based hybrid for potential

applications has been investigated extensively. Based on its unique properties, considerable efforts have been made to incorporate graphene into TiO_2-based hybrid materials.[21] Hence, several methods have been proposed to form TiO_2-decorated graphene (TiO_2-G) nanohybrids with graphene oxide (GO), such as UV-assisted reduction,[22] chemical and thermal methods.[23] But these methods are commonly complicated and high cost. Recently, Li's group prepared a TiO_2-G nanohybrid photocatalyst with GO and as-prepared TiO_2 (P25) using a facile one-step hydrothermal method, which showed a high photodegradation performance for methylene blue.[24] It should be noted that most of the P25 particles were observed along the edge and wrinkles than on the basal plane.

Herein, we first synthesized TiO_2-G nanohybrids with GO and tetrabutyl titanate, using a facile one-step solvothermal reaction. The nanohybrid could be produced directly from GO in a facile one-step reaction, where the reduction of GO and the deposition of TiO_2 on graphene occur simultaneously. Compared with the former methods,[22,23] this new process shortened the reaction steps. The individual TiO_2 NPs not only well decorated the surface of graphene sheets, but also prevented the graphene sheets from restacking. To the best of our knowledge, the AChE biosensor based TiO_2-G nanohybrids have not been developed. In an effort to develop a highly sensitive biosensing platform for OPs, we have explored the utilization of as-prepared TiO_2-G nanohybrids as an immobilization matrix. Due to the integrating of TiO_2-G nanohybrids, the immobilized AChE exhibited greater affinity to its substrate and excellent catalytic effect on the hydrolysis of ATCl. The enzyme-based biosensor was constructed for the rapid quantitative determination of carbaryl, a model of OPs. The proposed biosensor showed acceptable stability and sensitivity, and had potential application in AChE-inhibitors OPs analysis and environmental monitoring.

Experimental

Materials and reagents

Acetylcholinesterase (AChE, Type C3389, 500 U mg^{-1} from electric eel), acetylthiocholine chloride (ATCl) and carbaryl were purchased from Sigma-Aldrich (USA) and used as received. Graphite was purchased from Qingdao Tianhe Graphite Co., Ltd. Tetraethyl orthosilicate ($Si(OC_2H_5)_4$), and tetrabutyl titanate ($Ti(OC_4H_9)_4$) were purchased from Sinopharm Chemical Reagent Co., Ltd. 0.1 M phosphate buffer solution (PBS, pH7.0) was prepared by mixing stock standard solutions of NaH_2PO_4 and Na_2HPO_4, and adjusting the pH with 0.1 M NaOH. Unless otherwise stated, reagents were of analytical grade and used as received. All aqueous solutions were prepared with doubly distilled water.

Synthesis of TiO_2-G nanohybrids

Graphene oxide (GO) was prepared following the modified Hummers method[25] using purified natural graphite. The TiO_2-graphene (TiO_2-G) nanohybrid was synthesized as follows. Typically, the GO (34 mg) was dispersed into a solution (8.5 mL) that contained $Si(OC_2H_5)_4$, $Ti(OC_4H_9)_4$, and anhydrous ethanol at a volume ratio of 1 : 10 : 60. Then, the mixture of anhydrous ethanol (8.5 mL), 28% $NH_3 \cdot H_2O$ (0.8 mL), 30% H_2O_2 (8.5 μL) was added slowly to the first mixture and further stirred at room temperature until a gel was formed. The mixture was transferred into a 20 mL Teflon-sealed autoclave and heated at 170 °C for 30 h. After cooling to room temperature, the precipitate was collected by centrifugation and washed several times with deionized water and anhydrous ethanol. The washed precipitate was dried in a vacuum oven at 50 °C.

Electrode preparation and modification

Prior to modification, the glassy carbon electrode (GCE) was first polished with sand paper followed by 1.0, 0.3, and 0.05 μm alumina slurry, respectively. After successive sonication in ethanol and double distilled water, the electrode was rinsed with double distilled water and allowed to dry at room temperature. As displayed in Scheme 1, the modified electrode was prepared by a simple casting method as follows. Initially, the pretreated GCE was modified by dropping 6 μL 2.0 mg mL^{-1} TiO_2-G aqueous solution to fabricate the TiO_2-G modified GCE (denoted as TiO_2-G/GCE). The obtained electrode was finally coated with 4 μL AChE solutions, which were incubated at 25 °C for 30 min. After evaporation of water, the modified electrode was washed with PBS to remove the unbound AChE, and the resulting AChE-TiO_2-G/GCE was stored at 4 °C when not use. For comparison, AChE-TiO_2/GCE and AChE-G/GCE with the same quantities of AChE were prepared using the similar procedure.

Measurement procedure

Inhibition of OPs pesticides: the proposed AChE-TiO_2-G/GCE was first immersed in 0.1 M PBS containing different concentrations of standard carbaryl solution for 3 min and then transferred to the electrochemical cell of 5.0 mL PBS containing 0.4 mM ATCl to study the electrochemical response by cyclic voltammetry between 0.1 and 1.2 V (*versus* SCE). The inhibition of pesticide was calculated as follows: Inhibition (%) = $(1 - I_{p,exp}/I_{p,control}) \times 100$, where $I_{p,control}$ is the peak current of ATCl on AChE-TiO_2-G/GCE and $I_{p,exp}$ is the corresponding peak current of ATCl with pesticide inhibition.

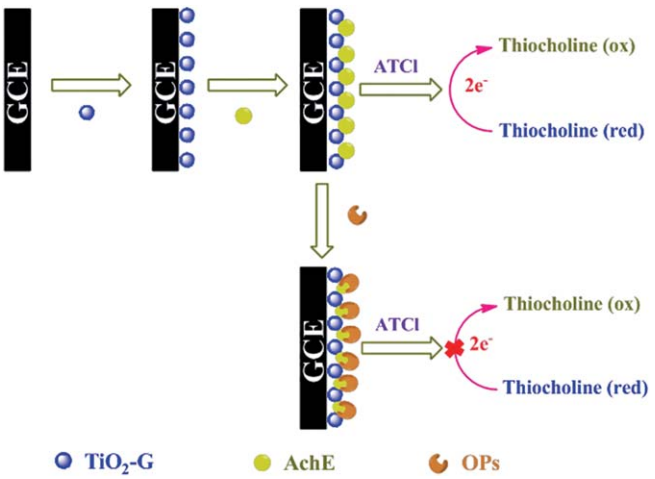

Scheme 1 Schematic representation of the biosensor fabrication and the principle for OPs determination.

The apparent Michaelis–Menten constant (K_m) of the biosensor: the typical current–time plot for the biosensor at 700 mV after the successive addition of ATCl to 0.1 M PBS with stirring. And then the K_m value, which gives an indication of the enzyme substrate kinetics for the biosensor, was determined by analysis of the slope and intercept for the plot of the reciprocals of the steady-state current *versus* ATCl concentration.

Instrumentation

The morphology of the as-prepared TiO_2-G nanohybrids was investigated using transmission electron microscopy (TEM, JEOL2100, Japan) and field-emission scanning electron microscopy (FE-SEM, Hitachi S4800, Japan). The IR spectra of the samples were obtained using an FT-IR spectrometer (Nicolet Nexus 470 FT-IR). Raman spectra were obtained on an RM 2000 microscopic confocal Raman spectrometer (Renishaw inVia Plus, England) employing a 514 nm laser beam. The electrochemical experiments were performed with a CHI660 B electrochemical analyzer (Chen Hua Instruments, Shanghai, China) with a conventional three-electrode system where a glassy carbon electrode (GCE, 3 mm in diameter) was used as working electrode, a saturated calomel electrode (SCE) as reference electrode and platinum wire as counter electrode, respectively. Electrochemical impedance spectroscopy (EIS) was performed in a 0.1 M KCl solution containing 5 mM $Fe(CN)_6^{3-/4-}$ with a frequency range from 0.01 Hz to 100 kHz at 0.24 V, and the amplitude of the applied sine wave potential in each case was 5 mV.

Results and discussion

Characterization of TiO_2-G nanohybrids

The morphology of the as-prepared TiO_2-G nanohybrid was investigated by employing SEM and TEM. As shown in Fig. 1a, it was obvious that the TiO_2-G nanohybrids had several layers, each of which exhibited TiO_2 NPs loading on all graphene surfaces. The TiO_2 NPs prevented the graphene sheets from restacking. The decoration of the 2D graphene sheet surface with the TiO_2 NPs also can be easily observed by TEM as shown in Fig. 1b. The individual TiO_2 NPs were well decorated on the graphene with a wrinkled paper-like structure. Most TiO_2 NPs had diameters of 5∼10 nm. The images demonstrated that the *in situ* preparation of TiO_2-G nanohybrids was effective for improving the morphology of TiO_2 NPs, and also showed the successful fabrication of TiO_2-G nanohybrids by one-step solvothermal reaction.

We investigated the as-prepared nanohybrid by FT-IR spectroscopy. As shown in Fig. 2A, several characteristic peaks of GO, in detail, the absorption due to C═O stretching of COOH groups situated at the edge of GO sheets was observed at about 1726 cm^{-1}. The peak at around 1623 cm^{-1} was assigned to the O–H bending vibration, and the absorption at 1396 cm^{-1} was attributed to tertiary C–OH groups,[26] while the absorption peaks at 1726 cm^{-1} and 1623 cm^{-1} of GO were not observed in the case of TiO_2-G. A new absorption band that appeared at 1570 cm^{-1} clearly showed the skeletal vibration of the graphene sheets.[27] The result confirmed the reduction of the GO sheets to graphene. In addition, TiO_2-G nanohybrids showed that the broad absorption at low frequency (below 900 cm^{-1}) was ascribed to the Ti–O–Ti structure,[28] similar to that in the spectrum of TiO_2. These characterizations proved the successful preparation of TiO_2-G nanohybrids.

Furthermore, to ascertain the reduction of GO to graphene, Raman spectra of GO and TiO_2-G were shown in Fig. 2B. Both

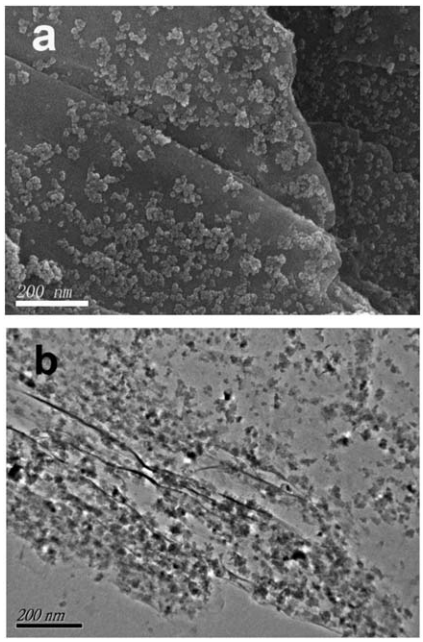

Fig. 1 (a) SEM image of TiO_2-G; (b) TEM image of TiO_2-G.

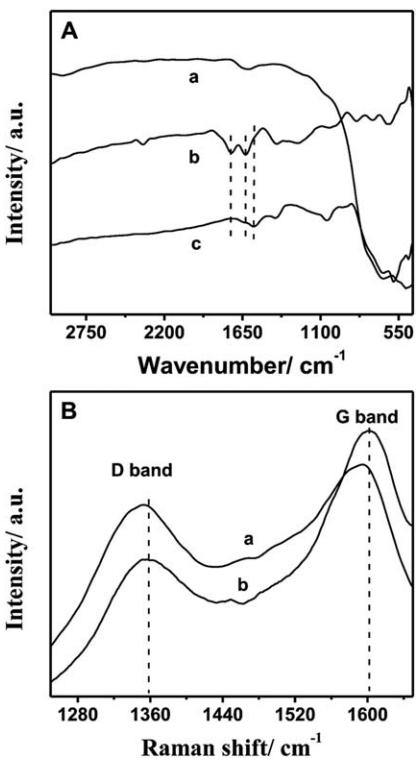

Fig. 2 (A) FT-IR spectra of (a) TiO_2, (b) GO, and (c) TiO_2-G; (B) Raman spectra of (a) TiO_2-G and (b) GO.

spectra showed the existence of the D band and G band. For GO, the G band was located at 1600 cm^{-1}, while for TiO_2-G nanohybrids, the G band moved to 1593 cm^{-1}, which was close to the value of the pristine graphite, indicating the reduction of GO during the solvothermal treatment. At the same time the existence of the D band at 1356 and 1348 cm^{-1} for both GO and TiO_2-G respectively predicted the defect of the sample and the size of the in-plane sp^2 domain.[29,30] The intensity ratio of the D and G band (I_D/I_G), changing from 0.71 to 0.90, indicated a slight increase in the average size of the sp^2 domain upon the reduction of GO by the solvothermal reaction. The studies of Stankovich *et al.*[31] and Paredes *et al.*[32] also found the similar result by chemical reduction for graphene.

EIS of the biosensor

EIS can provide useful information on the impedance changes of the electrode surface during the fabrication process.[33] The Nyquist plot of impedance spectra includes a semicircle portion and a linear portion, and the former at higher frequencies corresponds to the electron-transfer-limited process and its diameter is equal to the electron-transfer resistance.[34] By using the $K_3[Fe(CN)_6]/K_4[Fe(CN)_6]$ redox couple as an electrochemical probe, Fig. 3 exhibited the Nyquist plots of different electrodes in the frequency range from 10^{-2} to 10^5 Hz. It was obvious that the electron transfer resistance (R_{ct}) of the TiO_2-G/GCE was much lower than that of the bare GCE (curve a), and an almost straight line was exhibited (curve b). Here TiO_2-G immobilized on the electrode played an important role similar to an electron-conducting tunnel, making electron transfer to the electrode surface easier. After AChE was added on to the TiO_2-G/GCE surface, there showed a great increase in the diameter of the semicircle due to the increase of the thickness of the interface (curve c), which suggested that an enzyme layer formed an additional barrier and further prevented the redox probe to the electrode surface.[35] It was the direct evidence of successful binding of enzyme on the electrode surface.

Electrochemical behavior of AChE-TiO_2-G/GCE

Cyclic voltammetry (CV) was employed to evaluate the performance of the fabricated biosensor during stepwise modification. Fig. 4 presented the CV curves of different electrodes in the absence and presence of ATCl. No peak was observed at different electrodes in 0.1 M PBS. While 0.4 mM ATCl was added, an irreversible oxidation peak at 700 mV was observed at AChE-TiO_2-G/GCE (curve c), attributed to the oxidation of thiocholine, the hydrolysis product of ATCl catalyzed by immobilized AChE.[36] Furthermore, the peak current of AChE to ATCl on the AChE-TiO_2-G/GCE was much higher than that of the G/GCE and TiO_2/GCE, which was attributed to the presence of TiO_2-G nanohybrids with its inherent conductive properties can provide a conductive pathway for electron transfer.[37] Therefore, the TiO_2-G/GCE was utilized for OPs detection in our biosensing experiments.

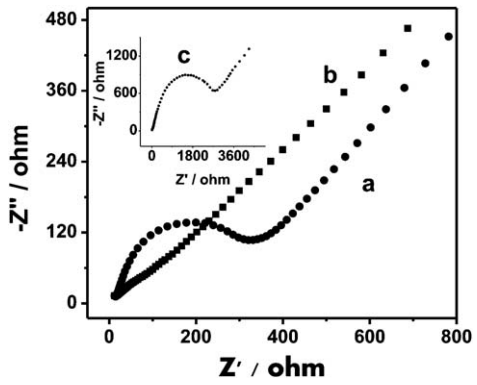

Fig. 3 EIS of (a) bare GCE, (b) TiO_2-G/GCE and (c) AChE-TiO_2-G/GCE in 0.1 M KCl containing 5 mM $K_3[Fe(CN)_6]/K_4[Fe(CN)_6]$.

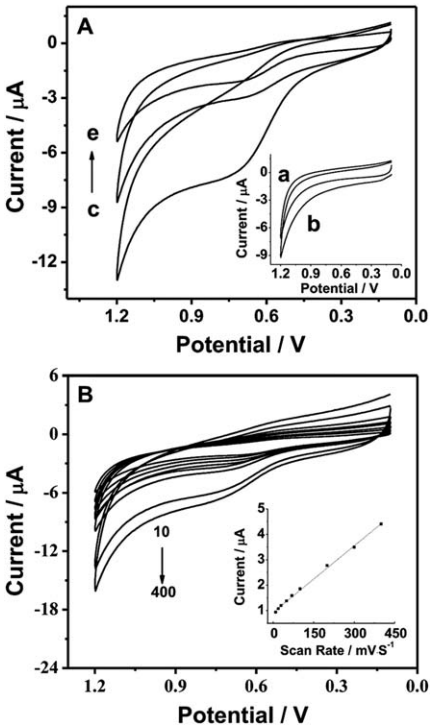

Fig. 4 (A) CVs of (a) bare GCE, (b) AChE-TiO_2-G/GCE in 0.1 M PBS (pH 7.0); (c) AChE-TiO_2-G/GCE, (d) AChE-G/GCE and (e) AChE-TiO_2/GCE in 0.1 PBS (pH 7.0) containing 0.4 mM ATCl. Scan rate: 50 mV s^{-1}. (B) CVs of AChE-TiO_2-G/GCE in 0.1 M PBS (pH 7.0) containing 0.4 mM ATCl at different scan rates from 10 to 400 mV s^{-1}. Inset: plots of peak current *vs.* scan rate.

Moreover, the effect of scan rate on the voltammetric response of immobilized AChE was also investigated. As displayed in Fig. 4B, with the increment of the scan rate, the peak current increases while the peak potential shifts slightly. The peak current exhibits a linear dependence on the scan rates ranging from 10 to 400 mV s^{-1} (inset in Fig. 4B), indicating a typical surface-controlled electrode process.[38]

Calibration plot of ATCl

The typical current–time response curve of the biosensor was obtained by successive additions of the substrate into a stirred cell. As displayed in Fig. 5A, with the increasing concentration of ATCl, the amperometric response increased linearly in the range of 0.3~1.1 mM with a correlation coefficient of 0.9987 and then

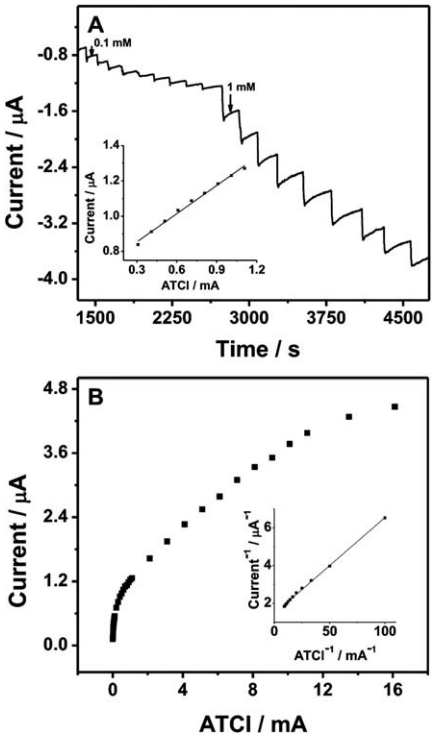

Fig. 5 (A) The amperometric *i–t* curve at the AChE-TiO_2-G/GCE for successive addition of ATCl with stirring at the applied potential of 700 mV. Inset: the calibration plot for ATCl determination. (B) The calibration plot for the ATCl sensor. Inset: the Lineweaver–Burk plot of $1/I_{ss}$ *vs.* $1/C$.

tended to a plateau value, showing a typical Michaelis–Menten process (Fig. 5B). The apparent Michaelis–Menten constant (K_m) is calculated to be 0.22 mM according to the Lineweaver–Burk equation. This value was much lower than that of AChE adsorbed on an AuNPs sol–gel film (0.45 mM),[37] a carbon nanotube *N*,*N*-dimethylformamide composite film (0.66 mM)[39] and a polyethyleneimine modified electrode (1.5 mM),[40] indicating that the immobilized AChE possessed a higher enzymatic activity and affinity for ATCl due to the excellent electron-transfer channels of TiO_2-G nanohybrids.[36]

Effect of incubation time on inhibition

In the pesticide analysis one of the most influential parameters is the inhibition time. Therefore, the dependence of incubation time on the carbaryl inhibition was also studied. As shown in Fig. 6, carbaryl displayed an increasing inhibition on AChE with the increase of immersion time, and when the incubation time was longer than 3 min, the curve trends to a stable value, indicating that the binding interaction with active target groups in the enzyme reaches saturation. However, the maximum value of inhibition was not 100%, which is likely attributed to the binding equilibrium between pesticides and binding sites in the enzyme.[38] Thus, a 3 min incubation time was used in subsequent experiments. This incubation time was obtained at a relatively small value (3 min) as compared to those reported multiwalled carbon nanotubes (MWCNTs) on an alkanethiol self-assembled monolayer modified Au electrode (8 min)[38] and Prussian blue-modified

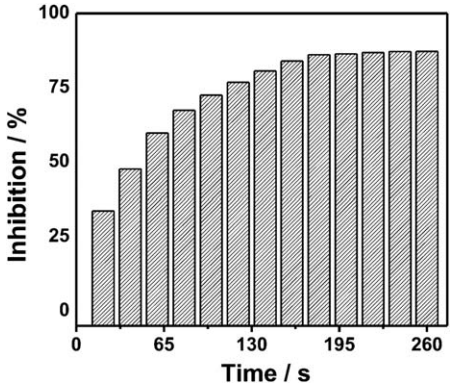

Fig. 6 Effect of the incubation time of pesticides on the AChE-TiO_2-G/GCE.

electrode (10 min).[1] To the best of our knowledge, such short inhibition time for OPs detection is rarely reported.

Detection of carbaryl

Based on the inhibition of OPs on the immobilized AChE activity, a simple and effective way for monitoring OPs was proposed. As shown in Fig. 7, the inhibition of carbaryl was proportional to its concentration from 0.001 to 0.015 μg mL^{-1} and from 0.015 to 2 μg mL^{-1} with a detection limit of 0.3 ng mL^{-1} (S/N = 3). The concentration range was wider than that of 66.4 ng mL^{-1} to 1.33 μg mL^{-1} for direct electrochemical determination of carbaryl using a multi-walled carbon nanotube/cobalt phthalocyanine modified electrode[41] and 10 ng mL^{-1} to 1 μg mL^{-1} by flow injection–direct chemiluminescence detection.[42]

Reactivation of the biosensor

It was also observed that the as-prepared biosensor inhibited by carbaryl within a certain concentration can resume 91.8% of its original value after immersion in 0.1 M PBS (pH 7.0) for 10 min, indicating that PBS plays an important role as a reagent for AChE reactivation. Compared with nucleophilic compounds such as pralidoxime iodide as a reagent of reactivation previously reported,[43] this method was simple and reliable.

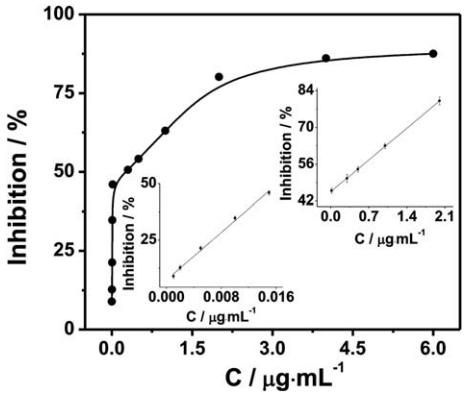

Fig. 7 Relationship between peak currents and concentrations of carbaryl. Insets: calibration plots for carbaryl determination.

Precision of measurements and stability of biosensor

The intra-assay precision of the biosensors was evaluated by assaying one enzyme electrode for five replicate determinations in 0.4 mM ATCl after being immersed in 0.01 μg mL^{-1} carbaryl for 2 min. Similarly, the inter-assay precision, or fabrication reproducibility, was estimated at four different electrodes. The RSD of intra-assay and inter-assay were found to be 6.3% and 8.2%, respectively, indicating an acceptable reproducibility.

The long-term storage stability was a critical issue for practical application of the proposed biosensor. When stored at 4 °C and measured at intervals over 2 days, no obvious decrease in the response of ATCl was observed in the first 7-day storage. After a 20-day storage period, the sensor retains 83% of its initial current response, indicating the acceptable stability of biosensor.

Conclusions

In summary, we have successfully constructed TiO_2-G nanohybrids *via in situ* growth of TiO_2 NPs on the surface of graphene sheets, which exhibited individual TiO_2 NPs well decorated on the surface of graphene sheets, preventing the graphene sheets from restacking. Serving as a biocompatible platform for enzyme immobilization, the proposed TiO_2-G nanohybrids provided a simple and efficient strategy for the immobilization of AChE and developed as a sensitive sensor for the rapid detection of carbaryl pesticide. Due to the excellent electron-transfer channels of the nanohybrid, the immobilized AChE possesses higher enzymatic activity and affinity to ATCl. A relatively short inhibition time was obtained by virtue of the TiO_2-G nanohybrids, which made the OPs carbaryl contact with the active site of AChE much easier and thus reducing the inhibition time. Based on the change in electrochemical response of enzymatic activity induced by OPs pesticide, an electrochemical technique with good reproducibility, acceptable stability and fast response for OPs pesticide was successfully developed. All of these good characteristics provide great promise for biosensor applications, which may open up new challenges and approaches to explore the electrochemical behaviors of graphene-based hybrids for other potential utilizations.

Acknowledgements

The present work is supported by the National Natural Science Foundation of China (No. 20875039 and 21075054), the Scientific Research Foundation of Jiangsu University (No. 06JDG016); Key Laboratory of Analytical Chemistry for Life Science (No. KLACLS07004), Key Laboratory of Modern Agriculture Equipment and Technology (No. NZ200809), Key Project on Basic Research of Educational Commission of Jiangsu Province of China (No. 10KJA470007), Research Fund for the Doctoral Program of Higher Education of China (No. 20093227110008).

References

1 X. Sun and X. Y. Wang, *Biosens. Bioelectron.*, 2010, **25**, 2611–2614.
2 J. M. Gong, L. Y. Wang and L. Z. Zhang, *Biosens. Bioelectron.*, 2009, **24**, 2285–2288.
3 A. Mulchandani, P. Mulchandani, I. Kaneva and W. Chen, *Anal. Chem.*, 1998, **70**, 4140–4145.
4 G. D. Liu and Y. H. Lin, *Anal. Chem.*, 2006, **78**, 835–843.
5 D. Du, J. W. Ding, J. Cai and A. D. Zhang, *J. Electroanal. Chem.*, 2007, **605**, 53–60.
6 D. Du, M. H. Wang, J. Cai and A. D. Zhang, *Sens. Actuators, B*, 2010, **146**, 337–341.
7 R. Sinha, M. Ganesana, S. Andreescu and L. Stanciu, *Anal. Chim. Acta*, 2010, **661**, 195–199.
8 P. V. Kamat, *J. Phys. Chem. Lett.*, 2010, **1**, 520–527.
9 H. Kim, A. A. Abdala and C. W. Macosko, *Macromolecules*, 2010, **43**, 6515–6530.
10 M. Pumera, A. Ambrosi, A. Bonanni, E. L. K. Chng and H. L. Poh, *TrAC, Trends Anal. Chem.*, 2010, **29**, 954–965.
11 Y. Y. Shao, J. Wang, H. Wu, J. Liu, I. A. Aksay and Y. H. Lin, *Electroanalysis*, 2010, **10**, 1027–1036.
12 C. S. Shan, H. F. Yang, D. X. Han, Q. X. Zhang, A. Ivask and L. Niu, *Biosens. Bioelectron.*, 2010, **25**, 1070–1074.
13 T. T. Baby, S. S. J. Aravind, T. Arockiadoss, R. B. Rakhi and S. Ramaprabhu, *Sens. Actuators, B*, 2010, **145**, 71–77.
14 R. S. Dey and C. R. Raj, *J. Phys. Chem. C*, 2010, **114**, 21427–21433.
15 K. Wang, Q. Liu, Q. M. Guan, J. Wu, H. N. Li and J. J. Yan, *Biosens. Bioelectron.*, 2011, **26**, 2252–2257.
16 R. B. Rakhi, K. Sethupathi and S. Ramaprabhu, *J. Phys. Chem. B*, 2009, **113**, 3190–3194.
17 F. H. Li, Z. H. Wang, C. S. Shan, J. F. Song, D. X. Han and L. Niu, *Biosens. Bioelectron.*, 2009, **24**, 1765–1770.
18 D. V. Bavykin, J. M. Friedrich and F. C. Walsh, *Adv. Mater.*, 2006, **18**, 2807–2824.
19 D. E. Gu, Y. Lu, B. C. Yang and Y. D. Hu, *Chem. Commun.*, 2008, 2453–2455.
20 L. C. Jiang and W. D. Zhang, *Electroanalysis*, 2009, **21**, 988–993.
21 C. Zhu, S. Guo, P. Wang, L. Xing, Y. Fang, Y. Zhai and S. Dong, *Chem. Commun.*, 2010, **46**, 7148–7150.
22 G. Williams, B. Seger and P. V. Kamat, *ACS Nano*, 2008, **2**, 1487–1491.
23 T. N. Lambert, C. A. Chavez, B. Hernandez-Sanchez, P. Lu, N. S. Bell, A. Ambrosini, T. Friedman, T. J. Boyle, D. R. Wheeler and D. L. Huber, *J. Phys. Chem. C*, 2009, **113**, 19812–19823.
24 H. Zhang, X. Lv, Y. Li, Y. Wang and J. Li, *ACS Nano*, 2010, **4**, 380–386.
25 S. Gilje, S. Han, M. H. Wang, K. L. Wang and R. B. Kaner, *Nano Lett.*, 2007, **7**, 3394–3398.
26 T. Szabó, B. Ottó, P. Forgó, K. Josepovits, Y. Sanakis, D. Petridis and I. Dékány, *Chem. Mater.*, 2006, **18**, 2740–2749.
27 C. Nethravathi and M. Rajamathi, *Carbon*, 2008, **46**, 1994–1998.
28 L. H. Lee and W. C. Chen, *Chem. Mater.*, 2001, **13**, 1137–1142.
29 W. Chen, L. Yan and P. R. Bangal, *Carbon*, 2010, **48**, 1146–1152.
30 S. Park, J. An, R. D. Piner, I. Jung, D. Yang, A. Velamakanni, S. T. Nguyen and R. S. Ruoff, *Chem. Mater.*, 2008, **20**, 6592–6594.
31 S. Stankovich, D. A. Dikin, R. D. Piner, K. A. Kohlhaas, A. Kleinhammes, Y. Jia and Y. Wu, *Carbon*, 2007, **45**, 1558–1565.
32 J. I. Paredes, S. Villar-Rodil, P. Solís-Fernández, A. Martínez-Alonso and J. M. D. Tascón, *Langmuir*, 2009, **25**, 5957–5968.
33 Y. Liu, R. Yuan, Y. Q. Chai, D. P. Tang, J. Y. Dai and X. Zhong, *Sens. Actuators, B*, 2006, **115**, 109–115.
34 X. H. Kang, J. Wang, H. Wu, I. A. Aksay, J. Liu and Y. H. Lin, *Biosens. Bioelectron.*, 2009, **25**, 901–905.
35 D. Du, W. Chen, W. Zhang, D. Liu, H. Li and Y. Lin, *Biosens. Bioelectron.*, 2010, **25**, 1370–1375.
36 D. Du, M. H. Wang, J. Cai, Y. H. Qin and A. D. Zhang, *Sens. Actuators, B*, 2010, **143**, 524–529.
37 D. Du, S. Z. Chen, J. Cai and A. D. Zhang, *Biosens. Bioelectron.*, 2007, **23**, 130–134.
38 D. Du, M. Wang, J. Cai, Y. Tao, H. Tu and A. Zhang, *Analyst*, 2008, **133**, 1790–1795.
39 A. Vakurov, C. E. Simpson, C. L. Daly, T. D. Gibson and P. A. Millner, *Biosens. Bioelectron.*, 2004, **20**, 1118–1125.
40 P. P. Joshi, S. A. Merchant, Y. D. Wang and D. W. Schmidtke, *Anal. Chem.*, 2005, **77**, 3183–3188.
41 F. C. Moraes, L. H. Mascaro, S. A. S. Machado and C. M. A. Brett, *Talanta*, 2009, **79**, 1406–1411.
42 G. Z. Tsogas, D. L. Giokas, P. G. Nikolakopoulos, A. G. Vlessidis and N. P. Evmiridis, *Anal. Chim. Acta*, 2006, **573–574**, 354–359.
43 D. Du, X. Huang, J. Cai and A. D. Zhang, *Sens. Actuators, B*, 2007, **127**, 531–535.

